Modelling the Dynamics of Craniofacial Growth

Jens Starke [a]

[a] *University of Heidelberg, Interdisciplinary Center for Scientific Computing & Institute of Applied Mathematics, Im Neuenheimer Feld 294,D-69120 Heidelberg, Germany,*
E-mail: Starke@iwr.uni-heidelberg.de

Jan Rübel [b]

[b] *University of Heidelberg, Interdisciplinary Center for Scientific Computing & Institute of Applied Mathematics, Im Neuenheimer Feld 294,D-69120 Heidelberg, Germany,*
E-mail: Jan.Ruebel@iwr.uni-heidelberg.de

Christopher J. Lux [c]

[c] *University of Heidelberg, Department of Orthodontics, Dental School, Im Neuenheimer Feld 400, D-69120 Heidelberg, Germany,*
E-mail: Christopher_Lux@med.uni-heidelberg.de

An analysis, visualization and modelling of the dynamics of craniofacial growth is presented, which is based on a Karhunen-Loève decomposition of time-discrete landmark data describing the craniofacial skeleton and its growth. This allows for a clear and suggestive depiction of craniofacial growth patterns and their dynamical behaviour, which is necessary for medical diagnosis as well as for orthodontic treatment. For modelling the dynamics, a medically motivated approach based on a dynamical system with general and individual parameters is used to obtain the underlying general growth laws. The parameters are identified by a least squares method for fitting the model to the growth data which consist of a rat calvarial data set and data of a human growth study. This allows for a quantitative description of the dynamics of size and shape changes as well as a qualitative prediction of growth processes.

Keywords: craniofacial growth, modelling growth and shape dynamics, Karhunen-Loève decomposition, numerical parameter identification in dynamical systems, least squares techniques, decomposition of the optimization problem

AMS Subject classification: 49M27, 90C90, 92C50, 92-08, 93B30, 65K05, 65K10

1. Introduction

In many medical or biological disciplines it is essential to understand and influence the growth of organisms. Growth mechanisms comprise both a major change in size and a minor one in shape. The change in shape of the craniofacial skeletal structures is of particular clinical interest in dentofacial orthopedics and surgery.

Many children show dental malocclusions or malrelationships of the jaws which may lead to severe functional and esthetic problems. A great number of them are induced by pathological craniofacial shape changes. Thus, the clinical aim is to diagnose and treat these developmental anomalies as early as possible to provide a coordinated development also with respect to a reduced need for surgical procedures. From the medical point of view a clear and suggestive depiction of craniofacial shape changes and growth patterns together with their dynamical behaviour is necessary for clinical diagnostics and treatment planning and has not been achieved satisfyingly yet. Hence an analysis based on a Karhunen-Loève decomposition (KLD) [22,26,12] of the time-discrete landmark data describing the craniofacial skeleton and its growth pattern is presented.

The visualization and modelling is based on the analysis of homologous landmarks, i.e. points which can be identified with sufficient precision on the x-rays. As the roentgenograms are rotated and translated to each other in the projection plane and do not have a common coordinate system, it is appropriate to use a data representation which is invariant under translation and rotation. For the present study we use the vector of all interpoint distances of landmarks. This representation is coordinate-free and does not have the disadvantage of traditional superimposition methods where the findings depend on the respective superimposition rule [29]. Moreover, many traditional cephalometric methods only measure a few specific angles for which different growth patterns may result in similar angular changes. In contrast to that, as also pointed out in [24,25] in the context of the Euclidean Distance Matrix Analysis (EDMA), the matrix of the Euclidean inter-landmark distances used here provides an appropriate data base to analyse the relative positional changes of cephalometric landmarks and to consider the object's entire geometry. The presented visualization technique uses coloured or patterned graphs to indicate shape changes and assigns either colours of a spectrum ranging from blue to red or patterned gray shades to the interpoint distances of the landmark configurations.

The Karhunen-Loève decomposition allows for a reduction of the dimension of the time-dependent data to a few spatial modes and their time-dependent scalar mode coefficients. This decomposition is closely related to principal components analysis. The reduction is necessary for an analysis and visualization as well as for a modelling of the growth processes. The time-dependent mode coefficients quantitatively describe the dynamics of size and shape components while the individual shape is covered by the spatial modes.

As the microscopic behaviour of the craniofacial skeletal growth is not known in detail, a phenomenological modelling is used for the growth dynamics. This is a medically motivated approach based on a dynamical system for the mode coefficients where general parameters are responsible for the qualitative properties of the flow and individual parameters account for the individual size and time scale. This is possible due to the property of the KLD to reduce the dimension of the time-dependent variables significantly. Fitting the parameters to the data determines the underlying general growth laws. The nonlinear parameters of the dynamical system are identified by a least squares method. In order to fit the model to the growth data, the error function is minimized by decomposing the parameter space into the subspaces of common linear and individual nonlinear parameters.

The determined ODE model of the mode coefficients allows for a qualitative prediction of growth processes by numerical integration of the initial value problem to enhance conventional subjective prediction approaches in dentofacial orthopedics. In order to capture individual growth laws, it is necessary to use a longitudinal study design, i.e. roentgenograms of the same individual at different ages. In the present paper craniofacial growth was analyzed for two data sets, namely rat calvarial data and human craniofacial data. They complement each other, because the rat data set comprises the records of a complete development, while the human data set focuses on a relatively short clinically relevant period of facial development.

1.1. Rat Calvarial Data

First, the rat calvarial data set of H. Vilman and M. L. Moss [28,5] is used, which comprises the longitudinal craniofacial growth of 18 rats, measured on lateral roentgenograms of the skull. In morphometric literature (for instance [5]) this data set turned out to be highly useful for the analysis of craniofacial

growth laws because it comprises all developmental stages beginning from birth to the adult state with final size and contains more time steps than most of the human growth studies. Thus, this rat calvarial data set was used in addition to the human data to develop the technique presented here. It comprises the landmark coordinates of 18 male rats measured on lateral cephalograms taken at 8 different stages from 7 to 150 days of age. The rat calvarial data set consists of the coordinates of 8 landmarks shown in Fig. 1, so that the resulting time-dependent vector of all interpoint distances has the dimension $8 \cdot 7/2 = 28$.

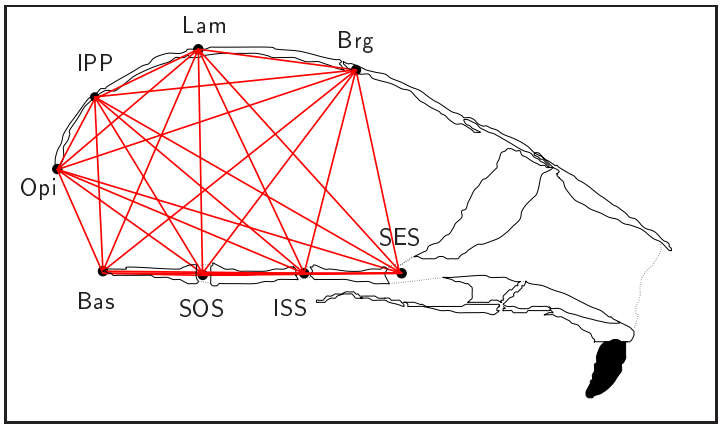

Figure 1. Midsaggital section of a rat skull showing the 8 landmarks used: Basion (Bas), Opisthion (Opi), Interparietal suture (IPP), Lambda (Lam), Bregma (Brg), Spheno-ethmoidal synchondrosis (SES), Intersphenoidal suture (ISS), Spheno-occipital synchondrosis (SOS) (after [5]). The graph represents the interpoint distances of the landmarks.

1.2. Belfast Growth Study

To get insight into the medically relevant growth processes of children, the laws and the developmental dynamic changes during human craniofacial growth were analysed on the basis of a longitudinal data set from the Belfast Growth Study. This large longitudinal European growth study started in 1960 and was carried out by C. P. Adams, University of Belfast [1]. It comprises X-rays from 300 children aged 5 in 1960 who were examined over a 10-year-period. Lateral cephalograms were obtained annually. As some of the 5 and 6 year old children did not have the teeth in occlusion during the x-ray, which impedes the analysis of the whole facial growth, the time interval 7 to 15 years was used in the present study. From the clinical point of view, this interval is highly useful because during

that period most medical growth-modifying procedures, such as orthodontic and orthopedic treatment, are carried out.

In the present study, 10 male subjects with suitable cephalometric records were included into the study. They exhibited after the eruption of all permanent teeth, except the third molars, a good occlusion of the teeth, i.e. no major orthodontically relevant anomalies. The 9 lateral cephalograms of each child, taken annually between 7 and 15 years of age, provide the data basis for the present study. First, the lateral cephalograms were scanned (600 dpi), and subsequently the coordinates of 7 cephalometric landmarks were determined.

The 7 landmarks sella (S), nasion (N), anterior and posterior nasal spines (ANS, PNS), gonion (Go), articulare (Ar) and gnathion (Gn), shown in Figure 2, were identified to assess the skeletal changes of maxilla, mandible and cranial base and their relative positional changes. It should be mentioned that articulare is not

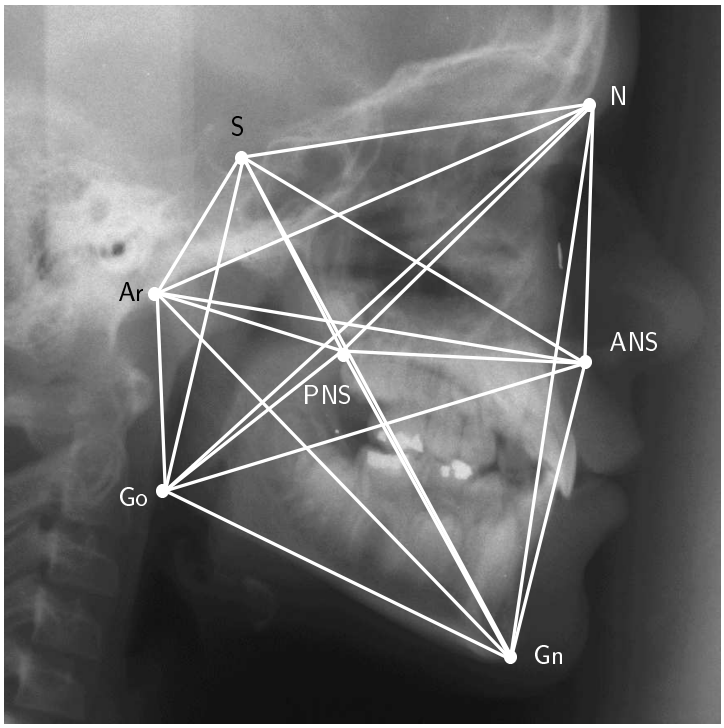

Figure 2. X-ray of a proband with age 13 years. The graph represents the interpoint distances of the used landmarks.

a real anatomical point. It is the (radiological) intersection of the ramus ascendens

of the mandible with the cranial base. These 7 landmarks are common in medical craniofacial analysis especially to assess skeletal changes, not changes of the teeth. The coordinates of the landmarks were used to calculate the $7 \cdot 6/2 = 21$ Euclidean interpoint distances.

2. Analysis of Growth Data and Visualization

To analyse and visualize the growth patterns of the high-dimensional and time-dependent growth data, a reduction of the dimension and decomposition into synchronous growth patterns is desirable. This is obtained by a Karhunen-Loève decomposition (KLD) which allows for a decomposition of the high-dimensional time-dependent data into a few time-dependent mode coefficients and corresponding spatial modes.

2.1. The Karhunen-Loève Decomposition

The Karhunen-Loève decomposition [22,26,12] is well known in data analysis and often used to reduce the degrees of freedom [38,39,21]. This property of reducing the dimension [12] is essential in the context of modelling to avoid having too many parameters in the model.

The KLD yields a separation of the data vector $q(t) \in \mathbb{R}^n$, given here as vector of the Euclidean interpoint distances, into time-dependent scalar coefficients $\xi_i(t) \in \mathbb{R}$ and pairwise orthogonal vectors, so-called modes $v^{(i)} \in \mathbb{R}^n$ which are independent of time. The modes are obtained by minimizing the error functional

$$F_k = \frac{1}{N} \sum_t \left\| q(t) - \sum_{i=1}^{k} \xi_i(t) v^{(i)} \right\|^2 \to \min \quad \forall k \tag{1}$$

with $N = \sum_t \|q(t)\|^2$ and the Euclidean norm $\|\cdot\|$. Variation of (1) with respect to $\xi_i(t)$ and $v^{(i)}$ leads to the eigenproblem $Cv^{(i)} = \lambda_i v^{(i)}$ where $C_{lm} = \frac{1}{N} \sum_t q_l(t) q_m(t)$ is the correlation matrix and $\lambda_i = v^{(i)T} C v^{(i)}$. To obtain the modes, this eigenproblem is solved numerically by a singular value decompostion [10,31] of the positive semi-definite symmetric matrix C representing the data. The coefficients are obtained by projecting the data vector onto the corresponding mode, i.e. $\xi_i(t) = q^T(t) v^{(i)}$. Using these modes, the relative error has the

form

$$\begin{aligned} F_k &= \frac{1}{N}\sum_t \left(\|q(t)\|^2 - 2\sum_{i=1}^{k} q(t)^T(\xi_i(t)v^{(i)}) + \sum_{i,j=1}^{k} \xi_i\xi_j v^{(i)T}v^{(j)} \right) \\ &= \frac{1}{N}\sum_t \|q(t)\|^2 - \frac{1}{N}\sum_t\sum_{i=1}^{k}\left(q(t)^T v^{(i)}\right)^2 = 1 - \sum_{i=1}^{k} v^{(i)T} C v^{(i)} \\ &= 1 - \sum_{i=1}^{k}\lambda_i. \end{aligned} \tag{2}$$

Thus, sorting the modes by the size of their eigenvalues yields the smallest error F_k for each number k of modes used for approximating the data. The present data sets show, like many others [20], that these ordered eigenvalues decrease strongly for the higher modes so that already a few modes yield a good approximation.

2.2. Visualization

To enhance comprehensibility for clinical practice, the modes of the KLD and the product of the mode coefficient and its corresponding mode are visualized by means of patterned and gray shaded graphs.

According to the value of the vector components to be visualized, different gray shades are assigned to the edges of the graph, representing the interpoint distances of the landmarks. These shades depict the components of the modes or the mode coefficients multiplied with their modes relative to the size of the corresponding data value, i.e. $v_j^{(i)}/\bar{q}_j$ and $\xi_i(t)v_j^{(i)}/\bar{q}_j$ respectively with the mean $\bar{q}$ over the time. In addition, different patterns are used for negative and positive values. Dashed lines are used for negative values while solid lines are used for positive ones. For each pattern, the shades range from white for zero to black for the extrema. The complete range of values and their visualization are shown in Fig. 3. The extrema of the values are $\pm\max_{i,j,k}\{|(b_{ij}(t_k))|\}$ where b_{ij} stands e.g. for $v_j^{(i)}/\bar{q}_j$ or $\xi_i(t_k)v_j^{(i)}/\bar{q}_j$ so that for each subject all modes i and discrete times t_k can be compared with each other. Nevertheless, it should be mentioned that coloured graphs, e.g. ranging from blue for negative values over white for zero to red for positive values are even more suggestive than the patterned gray shades which have been used here for technical reasons. The original positions of the landmarks are used as vertices of the graph for depiction. However, only the gray shaded edges of each graph are relevant for the analysis.

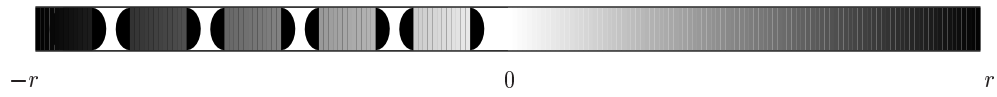

Figure 3. Patterned gray shades for the visualization of the results obtained by the KLD with $r = \max_{i,j,k}\{|(b_{ij}(t_k))|\}$ where b_{ij} stands e.g. for $v_j^{(i)}/\bar{q}_j$ or $\xi_i(t)v_j^{(i)}/\bar{q}_j$.

2.3. Analysis and Visualization of the Rat Calvarial Data

The KLD was carried out for each single subject of the rat calvarial data set. The rats show a major size change and a minor shape change. The first mode covers mainly changes in size while the second mode and, in finer approximations, also the remaining modes are responsible for the shape changes. The data set shows for each rat a characteristic dynamic behaviour of the first and second mode coefficient while the third one is already close to the measurement error. This hints to the existance of general growth laws for the first two modes and motivates the subsequent modelling of the corresponding dynamics.

Figure 4 shows the three KLD modes $v^{(1)}$ to $v^{(3)}$ with the largest eigenvalues (upper row) along with their time-dependent mode coefficients $\xi_1(t)$ to $\xi_3(t)$ (lower row) for rat no. 2. The modes decompose the growth processes into synchronous growth patterns which are linearly combined with the time-dependent mode coefficients. The uniform gray shades of the graph in the upper left picture in Figure 4 suggest that the first mode $v^{(1)}$ does not describe changes in shape, but a mere scaling of a kind of mean shape. This finding is also supported by the fact that for the present data the first mode coefficient shows a proportionality with an accuracy of $\pm 9.0 \cdot 10^{-3}$ to the so-called centroid size, a commonly used size measure in statistical shape analysis [5,11]. Thus, the shape components are represented by the remaining KLD modes, whose dynamic behaviour is given by the corresponding coefficients $\xi_i(t)$. The results of this decomposition allow for a better medical interpretation and simplify the analysis of the actual growth process. As already mentioned, this separation into spatial modes and time-dependent coefficients yields an appropriate basis for modelling the present growth behaviour with only a few parameters, which is shown in section 3.

For a better understanding of the synchronous anatomical processes described by the modes, the product $\xi_i(t)v^{(i)}$ of a mode and its amplitude has to be considered. Fig. 5 shows for rat no. 2 the product $\xi_2(t_k)v^{(2)}$ of the second

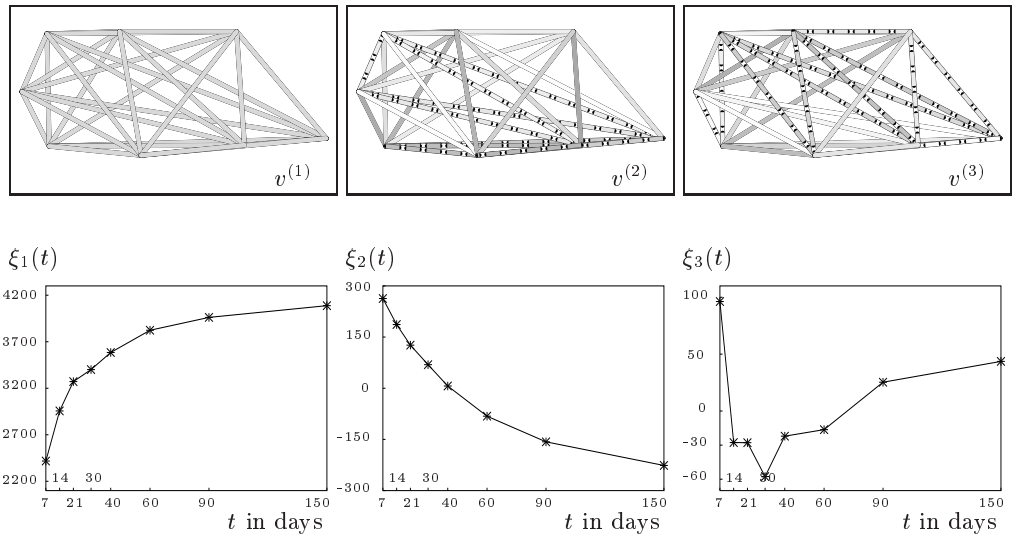

Figure 4. Modes v_1, v_2, v_3 of rat no. 2 of the rat calvarial data with the corresponding eigenvalues $\lambda_1 = 0.997532$, $\lambda_2 = 0.002139$, $\lambda_3 = 0.000180$ (upper row) and time-dependent mode coefficients $\xi_1(t)$ to $\xi_3(t)$ (lower row).

KLD mode and its amplitude on the left, which describes the major part of the shape component of the growth over time. This is compared to the entire shape component on the right of the figure. The gray shades indicate the contribution of this mode to the total length of the distance j, i.e. they are computed by $\xi_2(t_k)v_j^{(2)}/q_j(t_k)$. The negative contributions depicted in dashed lines do not indicate a shrinking of the distances but less growth in comparison to the scaling of the size represented by the first mode. For rat no. 2 in Fig. 5 the relative approximation error (2), computed by the eigenvalues of the correlation matrix, shows that the first mode covers 99.75% of the real process, the first and the second mode 99.97% and the first three ones cover 99.99%. Since the first mode describes the size, the complete shape component is represented by the sum $\sum_{i=2}^{n} \xi_i(t)v^{(i)}$ of the remaining modes, as visualized in Fig. 5 on the right. Comparing $\xi_2(t_k)v^{(2)}$ with $\sum_{i=2}^{n} \xi_i(t)v^{(i)}$ in the left and right columns in Fig. 5 it can be seen clearly that the second mode and its coefficient provide a good approximation of the entire shape component. This holds for all subjects of the rat calvarial data set where the approximation of the first two modes range from 99.961% to 99.981% with the mean 99.972%.

2.4. Analysis and Visualization of the Human Growth Data

The data of the Belfast Growth Study were investigated analogously to the rat calvarial data where the KLD was done separately for each subject. Although in the human data set a smaller developmental section is considered with a higher variability in shape, the results obtained for the analysis of the rat calvarial data also hold similarly for the data of the Belfast Growth study.

The first three KLD modes $v^{(1)}$ to $v^{(3)}$ with the largest eigenvalues together with their time-dependent mode coefficients $\xi_1(t)$ to $\xi_3(t)$ are given in Fig. 6 for proband no. 4. The different mechanisms of growth, especially with respect to the identification of regions with increased or decreased growth, can be clearly determined. Similarly to the rat calvarial data, the second mode together with its mode coefficient provides a good approximation of the real growth state also in the case of the Belfast Growth Study. Hence, a modelling of the growth dynamics can be restricted to the first two modes which cover for proband no. 4 for example 99.9952% of the real process and ranges over all probands from 99.9917% to 99.9953% with mean 99.9935%.

3. Modelling the Growth Dynamics

The property of the KLD to reduce the dynamics to a few time-dependent mode coefficients provides an appropriate basis for the modelling. It is important to fit a model with only a few parameters, i.e. the number of parameters has to be small compared to the amount of data to capture the common characteristic behaviour and prevent overdetermination.

3.1. Time Dependent Mode Coefficients for Modelling the Dynamics

As described above, the first two modes cover most of the real process and thus provide a sufficient approximation to model the dynamic growth behaviour. Their coefficients $\xi_1^p(t)$ and $\xi_2^p(t)$ are shown in Fig. 7 for each rat p. The similarity of the coefficient dynamics of each mode points to the existence of common growth laws for all subjects in the data set. The same observation can be made for the human growth study material in Fig. 8 with respect to the time-dependent coefficients of the first two modes. Although the human subjects show a larger relative variation in shifts of the subjects' graphs to each other, they seem to be

different segments of a general growth curve, which are scaled and translated to each other.

Previous approaches describe the fitting of certain growth curves, e.g. the growth curve of Jenss and Bayley [18] or of Gompertz [14] to nonlinear data of standing height or supine length in children [7,8]. For a detailed review of biological growth analysis the reader is referred to [40]. Besides traditional approaches measuring the dynamics of craniofacial variables, e.g. linear variables in lateral cephalograms [30], studies have been conducted to investigate the relationships between certain craniofacial variables, e.g. mandibular or maxillary dimensions, and skeletal growth in general as represented by total body size [2,6].

The dynamics of the nonlinear behaviour of human skeletal growth has been investigated in detail by Tanner [35,36,27] for standing height. Changes in human skeletal growth show after an initial strong growth a period of prepubertal decreased development and an increased growth during puberty, the so-called pubertal growth spurt. After this period the change in size tends to zero. The present data sets show a similar growth behaviour, which is pronounced for the human craniofacial data.

As already pointed out, the first mode $v^{(1)}$ represents a measure of size. Therefore, the dynamics of its mode coefficient $\xi_1(t)$ is assumed to show the growth behaviour described above. In mathematical terms, this is expressed by large (absolute) values of $\frac{d}{dt}\xi_1$ at the beginning, a subsequent local minimum which is followed by a local maximum and is zero at a final stationary state. This type of behaviour can be modelled by a gradient descent flow with polynomial potential of order four. Such a potential Φ with suitable coefficients, supplying the desired behaviour of the corresponding gradient flow, is depicted in Fig. 9.

The gradient flow dynamics with potential of order four, representing a general growth law, can be adapted to the individual by introducing the parameter α_1^p for each individual p to consider its individual time scale and parameters β_1^p and γ_1^p to consider the individual size at the initial and final state. This leads to the following equation of motion with $\tilde{\xi}_1^p$ for modelling the data ξ_1^p:

$$\begin{aligned}\frac{d}{dt}\tilde{\xi}_1^p &= f_1^p(\tilde{\xi}_1) \\ &= \alpha_1^p\left(k_{10} + k_{11}(\beta_1^p\tilde{\xi}_1^p - \gamma_1^p) + k_{12}(\beta_1^p\tilde{\xi}_1^p - \gamma_1^p)^2 + k_{13}(\beta_1^p\tilde{\xi}_1^p - \gamma_1^p)^3\right) \quad (3)\end{aligned}$$

with general parameters $k_{10}, k_{11}, k_{12}, k_{13}$ determining the qualitative properties like basins of attraction and stability and individual parameters α_1^p, β_1^p, γ_1^p. As-

suming such a general growth law which is adapted to the individual by the three introduced parameters allows for a much better fit of the general behaviour than by using more general and no individual parameters. Moreover, the assumption of a general growth law which combines general and individual parameters reduces the total number of parameters compared to the case of an individual parameter fit for every subject.

For the modelling of the second mode we assume that in growth processes any change in shape is accompanied by an increase in size, which is usually justified by the nature of craniofacial growth. To model the dynamics of the coefficient ξ_2^p of the second mode $v^{(2),p}$ representing the major component of shape, the following formulation with $\tilde{\xi}_2^p$ is used:

$$\begin{aligned} \frac{d}{dt}\tilde{\xi}_2^p &= f_2^p(\tilde{\xi}_1, \tilde{\xi}_2) \\ &= \left(\frac{d}{dt}\tilde{\xi}_1^p\right) \cdot g(\tilde{\xi}_2^p) \end{aligned} \tag{4}$$

with the quadratic function

$$g(\tilde{\xi}_2^p) = \alpha_2^p \Big(k_{20} + k_{21}(\beta_2^p \tilde{\xi}_2^p - \gamma_2^p) + k_{22}(\beta_2^p \tilde{\xi}_2^p - \gamma_2^p)^2 \Big). \tag{5}$$

Here α_2^p, β_2^p, γ_2^p are as in eq. (3) parameters to adapt the collective law to the individual. The parameter α_2^p adapts the shape changes covered by the second mode to the individual time scale while β_2^p and γ_2^p describe the individual markedness of shape comprised in the total growth. The specific form of (5) can be explained as follows: Due to the approximation of the growth data by a scaling of the first mode as a kind of mean shape with the scaling factor $\xi_1^p(t)$, and under the assumption of monotonous growth, the coefficient $\xi_2^p(t)$ changes its sign over time. It describes along with the second mode the deviations of the data from the first mode. Furthermore, it is clinically known that many shape characteristics develop during the pubertal growth spurt, and that in conclusion those characteristics are weakly expressed before puberty during the prepubertal minimum [3]. In addition, the facial skeleton tends to its final shape after puberty. This approximately sigmoidal and monotonous growth behaviour of ξ_2^p over time (cf. Figs. 7 and 8) is reflected in the quadratic dependence of $g(\tilde{\xi}_2^p(t))$ from $\tilde{\xi}_2^p(t)$. Within the range between the zeros of $g(\tilde{\xi}_2^p(t))$, the described behaviour is achieved under the stability conditions discussed in section 3.5.

3.2. Parameter Identification in the ODE Model

To complete the modelling of the growth dynamics for the rats and humans, the parameters in (3) and (4) have to be determined from the two data sets. One possible approach for a parameter identification in ordinary differential equations is to determine the parameters by minimizing the error between the solution of the differential equation and the data. Examples are the initial value approach [34] or multiple shooting [9,4,19]. The initial value approach starts from an initial guess for the parameters and the dynamic variable. It minimizes the error by iterating the determination of the parameters and initial value respectively and the numerical solution of the differential equation. In opposite to that, the method of multiple shooting not only uses the information of the flow for the initial value but on the whole fitting interval by dividing this interval in many subintervals and solving an initial value problem on each subinterval. The initially obtained discontinous solutions which are nevertheless close to the real data, are iteratively smoothed by adding equality constraints for the continuity conditions to the original optimization problem. An application example for multiple shooting for the parameter identification in an ODE model of a chaotic circuit can be found in [37].

In the following, another approach is used for the parameter identification, where the flow of the dynamical system is directly fitted to the data. This allows to utilize the specific structure of the parameters in the proposed model (3) and (4). Furthermore, it should be kept in mind, that this model is essentially based on a gradient descent flow which has a good-natured dynamics where perturbations in the parameters do not effect the trajectories too much. Both, the general and individual parameters are determined by fitting the flow of this ODE model to the data $\Delta\xi_i^p(t_k)/\Delta t$, while the general parameters are linear parameters and the individual parameters are nonlinear. As in the present x-rays the time measurement error is negligible compared to the error in identification of landmarks, the standard least squares method can be used instead of the total least squares method. This leads to minimizing the residuals

$$R_i(k_{ij}, \alpha_i^p, \beta_i^p, \gamma_i^p) = \sum_p \sum_k \left(\frac{\Delta\xi_i^p(t_k)}{\Delta t} - f_i^p(\xi_i^p(t_k)) \right)^2 \tag{6}$$

for each mode coefficient ξ_i^p given from the data with $i \in \{1, 2\}$, i.e.,

$$R_i(k_{ij}, \alpha_i^p, \beta_i^p, \gamma_i^p) \to \min . \tag{7}$$

Due to the large number of local minima it is quite difficult to find the global minimum of (6).

By using a decomposition method (see e.g. [13]) for minimizing (6), advantage is taken of the special structure of the optimization problem (6) with (7) where the general parameters k_{ij} are linear in the model (3) and (4) while the individual parameters α_i^p, β_i^p and γ_i^p appear nonlinearly. The residuals of the two decomposition steps are first

$$R_i^{(a)}(k_{ij}) = \sum_p \sum_k \left(\frac{\Delta \xi_i^p(t_k)}{\Delta t} - f_i^p(\xi_i^p(t_k); k_{ij}) \right)^2 \quad \text{while all} \quad \alpha_i^p, \beta_i^p, \gamma_i^p \quad \text{are constant} \tag{8}$$

for each mode coefficient ξ_i^p given from the data with $i \in \{1, 2\}$ for optimizing the linear general parameters k_{ij} and second

$$R_{i,p}^{(b)}(\alpha_i^p, \beta_i^p, \gamma_i^p) = \sum_k \left(\frac{\Delta \xi_i^p(t_k)}{\Delta t} - f_i^p(\xi_i^p(t_k); \alpha_i^p, \beta_i^p, \gamma_i^p) \right)^2 \quad \text{while all} \quad k_{ij} \quad \text{are constant} \tag{9}$$

for each mode coefficient ξ_i^p for optimizing the individual parameters $\alpha_i^p, \beta_i^p, \gamma_i^p$ for each proband p.

Minimizing (8) to determine the general parameters k_{ij} yields the global optimum due to the fact that they appear linearly in the model which has to be fitted to the data, i.e., they are quadratically in (8), with α_i^p, β_i^p and γ_i^p being fixed. Therefore, it is not crucial which optimization method is used for this step. In contrast to that, the individual parameters α_i^p, β_i^p and γ_i^p appear nonlinear in the model which has to be fitted to the data. To find subsequently suboptimal values for these individual parameters, a conjugate gradient method was carried out once with the parameter values of the previous step and $n_r = 128$ times with randomly chosen initial values. This was done independently for each proband with the general parameters k_{ij} being fixed. The best solution is used for the following iteration steps. Due to the low dimension of this search space compared to the original non-decomposed problem (6) there is a much higher chance to obtain the global minima of the residuals (9) for each subject p. The optimization of these two residuals (8) and (9) are iterated using the methods described above. As each of the steps decreases or at least does not increase the residual (6), the total procedure monotonously decreases the residual (6).

3.3. Fitting the Parameters for the Rat Calvarial Data

To further reduce the number of free parameters, in (3) and (4) the individual parameter γ_i^p with $i = 1, 2$ was chosen fixed as the mean amplitude $\gamma^p = \bar{\xi}_i$ of the ith mode over all rats and times. This is possible because all subjects of the rat calvarial data cover the whole growth period starting from birth [33]. Besides the mentioned advantage of the proposed model (3) to cover the characteristic behaviour better by using general and individual parameters, another benefit concerning the number of parameters should be mentioned: In the rat calvarial data set only $4+18\cdot 2$ parameters have to be determined instead of $18\cdot 4$ parameters for fitting the growth law individually to each subject. The time derivatives of the mode coefficients describing the growth data are calculated as difference quotients

$$\frac{\Delta\xi_i(t_{k+1})}{\Delta t} = \frac{\xi_i(t_{k+1}) - \xi_i(t_k)}{t_{k+1} - t_k} \tag{10}$$

from the growth data.

The fit for the rat calvarial data set yields the results for the parameters shown in Table 1 by using the described decomposition approach for minimizing (6). Fig. 10 shows the fit of the model (3) and (4) for rat no. 2.

Parameters for the first mode coefficient $\xi_1(t)$			
$k_{10} = 1.73$	$k_{11} = -2.76$	$k_{12} = 3.44$	$k_{13} = -5.58$
$\alpha_1^p \in [0.0057, 0.011]$	$\beta_1^p \in [0.98, 1.01]$	$\gamma_1^p = \bar{\xi_1} = 3.082$	
Parameters for the second mode coefficient $\xi_2(t)$			
$k_{20} = -0.41$	$k_{21} = 0.17$	$k_{22} = 7.29$	
$\alpha_2^p \in [0.81, 1.37]$	$\beta_2^p \in [0.81, 1.57]$	$\gamma_2^p = \bar{\xi_2} = 0.021$	

Table 1
Results of the parameter fit for the rat calvarial data.

3.4. Fitting the Parameters for the Belfast Growth Study

In contrast to the preceding section, in the model for the Belfast Growth Study γ_i^p was chosen as free parameter for the parameter fit. It describes the individual size for $i = 1$ and shape markedness for $i = 2$. The time derivatives of

the mode coefficients describing the given growth data are calculated as smoothed difference quotients

$$\frac{\Delta\xi_i(t_k)}{\Delta t} = \frac{1}{2}\left(\frac{\xi_i(t_{k+1}) - \xi_i(t_k)}{t_{k+1} - t_k} + \frac{\xi_i(t_k) - \xi_i(t_{k-1})}{t_k - t_{k-1}}\right) \tag{11}$$

from the growth data. This diminishes the number of sign changes in $\Delta\xi_i(t_k)/\Delta t$ which are based on fluctuations of the measurements. The obtained parameters are given in Table 2 while Fig. 11 shows the fit of the model (3) and (4) to the

Parameters for the first mode coefficient $\xi_1(t)$			
$k_{10} = 0.306$	$k_{11} = 0.563$	$k_{12} = 0.415$	$k_{13} = -1.146$
$\alpha_1^p \in [0.138, 0.306]$	$\beta_1^p \in [1.335, 3.215]$	$\gamma_1^p \in [4.184, 11.194]$	
Parameters for the second mode coefficient $\xi_2(t)$			
$k_{20} = -0.581$	$k_{21} = 4.092$	$k_{22} = 96.431$	
$\alpha_2^p \in [0.317, 16.700]$	$\beta_2^p \in [-1.100, 1.292]$	$\gamma_2^p \in [-0.054, 0.101]$	

Table 2
Results of the parameter fit of the Belfast Growth Study.

Belfast growth data of proband no. 4.

3.5. Qualitative Properties of the Obtained Growth Dynamics

As the proposed model is essentially based on a gradient descent flow, or at least can be transformed to one in the region of interest, the qualitative properties of the dynamics are simple. Most important are the stability properties which have to be fulfilled to ensure that only medically possible solutions appear.

The vector field

$$\begin{aligned} v(\xi_1^p, \xi_2^p) &= \begin{pmatrix} f_1^p \\ f_2^p \end{pmatrix} \\ &= \begin{pmatrix} \alpha_1^p\Big(k_{10} + k_{11}(\beta_1^p\xi_1^p - \gamma_1^p) + k_{12}(\beta_1^p\xi_1^p - \gamma_1^p)^2 + k_{13}(\beta_1^p\xi_1^p - \gamma_1^p)^3\Big) \\ f_1^p\alpha_2^p\Big(k_{20} + k_{21}(\beta_2^p\xi_2^p - \gamma_2^p) + k_{22}(\beta_2^p\xi_2^p - \gamma_2^p)^2\Big) \end{pmatrix} \end{aligned} \tag{12}$$

defines the dynamical system $(\dot{\xi}_1^p, \dot{\xi}_2^p)^T = v(\xi_1^p, \xi_2^p)$ with (3), (4) and the parameters given in Tables 1 and 2. Its flow is qualitativly shown in Fig. 12. The

individual parameters α_i^p, β_i^p and γ_i^p do not change the flow of (13) if $\alpha_i^p > 0$ for $i = 1, 2$ and $\beta_1^p > 0$. The regions A and D in the phase portrait represent medically impossible states while the region C is avoided by sign convention. More precisely, trajectories in D would correspond to shrinking. Trajectories in A would diverge which makes no sense with respect to the nature of growth. This area is avoided by the assumption of non-monotonous behaviour of the shape.

4. Qualitative Prediction of Craniofacial Growth

Many treatment decisions depend on the prediction of the craniofacial growth pattern, especially the growth direction of the mandible. In clinical practice a rough prediction is based on some structural signs [3] such as the morphology of the symphysis or some angular measurements describing the position of the jaws relative to the skull. However, so far the existing approaches are of limited clinical use [16,23]. Nevertheless, prediction is of great importance in clinical treatment planning. If x-rays at several developmental stages are available, e.g. in cases with severe syndroms where patients are x-rayed over a larger period of craniofacial development, the available data might cover the relevant growth tendencies necessary for prediction. Thus, the prediction as follows may to a limited extent assist the clinician to determine and at least qualitatively predict the effects of the existing growth trends on craniofacial morphology.

An estimation of the future growth can be performed by numerical integration of the extracted growth laws, using for the dynamical system the general parameters and the mean of the individual parameters obtained above. While the general parameters describe the characteristic shape of the growth curve which contains the medically relevant information, the individual parameters adapt the individual time scale and absolute size. The prediction by numerical integration is performed by applying the determined growth laws to new individual Karhunen-Loève modes. These modes are obtained from those time steps which are available for prediction. To be precise, the final values of the first two mode coefficients determined by the available data are used as initial values for the integration of the dynamical system.

The prediction state is

$$\tilde{q}(t) = \tilde{\xi}_1(t)\tilde{v}^{(1)} + \tilde{\xi}_2(t)\tilde{v}^{(2)} \tag{13}$$

where $\tilde{v}^{(1)}, \tilde{v}^{(2)}$ are the KLD modes of the available data and $\tilde{\xi}_1(t), \tilde{\xi}_2(t)$ the cor-

responding coefficients obtained by the numerical integration of the ODE model capturing the growth law.

4.1. Prediction for the Rat Calvarial Data

The capability of this prediction approach is first shown for the rodent data. To evaluate the prediction result, only two states at times t_4 and t_5 of the original data set with the times t_1 to t_8 were used as basis for the prediction. The predicted subsequent states $\tilde{q}$ were compared with the states q after real growth. The KLD modes of the subset approximate the modes of the original data set including the states to be predicted.

To integrate the model (3) and (4) for prediction, the mode coefficients $\xi_1(t_5)$ and $\xi_2(t_5)$ which correspond to the modes of the subset are used as initial values. Using Euler's method for numerical integration, good results are obtained for the first mode and satisfying qualitative results for the second mode. Fig. 13 shows that the main shape effects captured by the second mode are qualitatively well predicted by the proposed model. In the figure one can see that the relative elongation (dark solid lines) of the distances Bas–SES, Bas–SOS and SOS–ISS and the relative compression (dark dashed lines) of the vertical distances (Bas–Opi and SOS–Lam) are predicted correctly. Therefore, a qualitative estimation of the future tendencies of growth seems possible. The prediction error in the right column shows for t_5 the initial difference between the second mode computed over all time steps t_1 to t_8 and the second mode computed over t_4 and t_5. The prediction error of the other times is therefore a combination of a propagation of this error and the approximation error of the model. Due to the individual time and length scales, the decisive point here is to capture the directions of the changes of certain growth regions qualitatively, regardless the exact quantitative values.

4.2. Prediction of Human Craniofacial Growth

To test the predictive capabilities in a clinical setting, the x-rays at 7 to 13, 9 to 11 and 11 to 13 years have been used to predict the interlandmark distances in the respective two subsequent years. Additionally one of the 10 subjects was excluded from the parameter estimation procedure to test the capability of this prediction on subjects not in the data base.

For all time intervals which were used for prediction, most of the qualitative shape changes were predicted correctly for the 10 subjects. The prediction results of the distance vectors were of a quality (see Table 3) that seems to make these results useful for medical prediction. Nevertheless, the prediction error of the

pred. basis	7–13		9–11		11–13	
pred. age	14	15	12	13	14	15
rel. total error	1.8%	3.6%	2.0%	1.9%	2.2%	2.3%
stand. dev. of total error	0.0045	0.0087	0.0089	0.0051	0.0050	0.0049

Table 3
Mean of relative errors of the prediction $\tilde{\xi}_1(t)\tilde{v}^{(1)} + \tilde{\xi}_2(t)\tilde{v}^{(2)}$, for the basis of ages 7–13, 9–11 and 11–13, over all subjects and corresponding standard deviations.

second mode is relatively high which makes possible only a qualitative prediction of the shape change.

In Fig. 14 $\xi_2(t)v^{(2)}$ of the real growth has been opposed to $\tilde{\xi}_2(t)\tilde{v}^{(2)}$ of the prediction result. The data for ages 11–13 were used as basis for the prediction. As in the preceding section the prediction error is a combination of an initial error due to the approximation of the data base over the times t_5 to t_9 by the reduced data base over the times t_5 to t_7 and an error coming from the model assumptions. Although the prediction error seems to be large, the growth behaviour of most regions is predicted qualitatively correct. Indeed, the relatively long posterior facial height S–Go and distance Ar–Go and the relatively shortened anterior facial height (N–Gn), distances which are essential for the craniofacial growth pattern, are predicted qualitatively correct. The relative changes of the real growth and the prediction, together with the prediction error as their difference, are visualized in Fig. 15. This prediction error is small compared with the relative changes of the real growth.

In a second step, the growth of a proband, who has not been included in the data set which was used to determine the parameters of the model, is predicted in Fig. 16. The means determined over the 9 remaining subjects were used as individual parameters. Prediction results were shown for the age 15 on a basis of the ages 7 to 14. For the prediction, different individual time scales $\alpha_2 = \{\bar{\alpha}/16, \bar{\alpha}/4, \bar{\alpha}/2, \bar{\alpha}\}$ with mean $\bar{\alpha} = 3.180$ were used because the

individual time scale is not known and also not of major medical relevance. For better visualization, the gray scale was determined over each row of Fig. 16 separately. It has to be mentioned that the mean $\bar{\alpha}$ is relatively high due to a very large parameter value of one proband. The growth pattern of the second mode is qualitatively well predicted. The quantitatively best prediction is given for $\alpha_2 = \bar{\alpha}/16$.

On the other hand it should be mentioned that the fundamental limits of any approach of craniofacial growth prediction have to be seen clearly. If the prediction is based solely on cephalometric measurements of a single state it is principally not possible to predict sudden changes of the growth direction without further genetic information [15,17]. For a quantitatively correct prediction at least some tendencies have to be present for several time steps in the data set on which the prediction is based. Over and above that, it has to be emphasized that the number of x-rays usually available for an estimation of the future growth is very limited in clinical practice. Most treatment decisions have to be made when the patient comes for the first time into practice, i.e. growth has to be predicted on the basis of only one x-ray in lateral view.

The need of a certain number of cephalometric x-rays necessary for prediction with high accuracy contrasts to the increasing sensitivity towards ionizing radiation and this discrepancy may perhaps be solved in future by the further development and adaption of existing diagnostic techniques such as ultrasound or magnetic resonance tomography to craniofacial diagnostics.

5. Conclusions and Outlook

A technique based on a Karhunen-Loève decomposition is presented to investigate and visualize landmark-based data of time-dependent processes. This approach turned out to be a suitable tool for analysing, visualizing and modelling complex growth mechanisms and has been exemplarily demonstrated in the context of craniofacial growth.

The growth processes, represented by time-dependent interpoint distances of landmark data, are decomposed into time-dependent scalar mode coefficients and spatial modes which are constant over time. The investigated data sets comprise first, the rat calvarial data set of Vilman [28,5] and second, a group of male subjects from the Belfast Growth Study [1]. They show that already the first two modes approximate the growth process with high accuracy and represent the

dynamics of size and shape components during growth. Thereby, the first mode covers mainly the increase in size while the second one describes the main shape component.

The presented technique allows for a visualization of the growth processes which is suggestive and self-evident for medical use due to colouring or gray shading of the time-dependent interpoint distances of the landmark data. The used patterned gray shades depict the effects of the modes on the different craniofacial regions. For example, the second mode shows in certain regions a decrease or increase compared to the mean growth covered by the first mode, which is depicted with dashed or solid lines.

In contrast to approaches common in medical cephalometric analyses which only use some angular measurements to describe shape change, the object's whole geometry is under consideration, which is mainly the neurocranium for the rats and the facial skull for the Belfast Growth Study. This is a clear advantage over conventional cephalometric analyses, where the geometric relationships among certain measurements, e.g. the fact that they share a common landmark, is not taken into account [32]. In the decomposition into spatial modes and time-dependent coefficients as described above, the mode coefficients give insight into the individual dynamic behaviour during the observed growth period, i.e. the entire development in the case of the rats and the period of starting puberty and adolescence for the Belfast subjects. Furthermore, the reduction of the dynamics to a few time-dependent scalar mode coefficients allows for an extraction of general growth laws. A medically motivated dynamical system with general and individual parameters was used to model and predict the complex growth processes qualitatively. For the parameter identification in the dynamical system, a least squares technique with a decomposition method for minimizing the residual error was used. Besides the existing traditional approaches [30], [2], [6] for modelling the dynamics of size measures like linear craniofacial distances, the presented model includes the dynamics of shape characteristics as well.

In future, the adaptation to three-dimensional data, necessary for the analysis of computer tomographies, is also possible because the KLD is not limited to two dimensions. The development of new diagnostic techniques without or with at least strongly reduced ionizing radiation would allow to take a distinctly larger number of cephalometric pictures during development or treatment. This would facilitate modelling and prediction with higher accuracy and might also allow for a better quantitative prediction of growth processes in medical diagnostics.

References

[1] C. P. Adams. Changes in occlusion and craniofacial pattern during growth. *European Orthodontic Society Transactions*, pages 85–96, 1972.

[2] B. Baughan, A. Demirjian, G. Y. Levesque, and L. Lapalme-Chaput. The pattern of facial growth before and during puberty, as shown by french-canadian girls. *Annals of Human Biology*, 6(1):59–76, 1979.

[3] A. Björk. Prediction of mandibular growth rotation. *American Journal of Orthodontics*, 55:585–599, 1969.

[4] H. G. Bock. Randwertproblemmethoden zur Parameteridentifizierung in Systemen nichtlinearer Differentialgleichungen. *Bonner Mathematische Schriften*, 183, 1987.

[5] F. L. Bookstein. *Morphometric Tools for Landmark Data: Geometry and Biology.* Cambridge University Press, 1991.

[6] P. H. Buschang, R. M. Baume, and G. G. Nass. Craniofacial growth and size patterns during postnatal development. *Growth*, 47, 1983.

[7] J. Deming. Application of the Gompertz curve to the observed pattern of growth in length of 48 individual bioys and girls during the adolescent cylcle of growth. *Human Biology*, 29:83–122, 1957.

[8] J. Deming and A. H. Washburn. Application of the Jenss curve to the observed pattern of growth during the first eight years of life in forty boys and forty girls. *Human Biology*, 35:484–506, 1963.

[9] P. Deuflhard. A modified newton method for the solution of ill-conditioned systems of nonlinear equations with applications to multiple shooting. *Numerische Mathematik*, 22:289–311, 1974.

[10] P. Deuflhard and A. Hohmann. *Numerische Mathematik Bd. 1.* de Gruyter, 1993.

[11] I. L. Dryden and K. V. Mardia. *Statistical Shape Analysis.* Wiley, 1998.

[12] A. Dür. On the optimality of the discrete karhunen-Loève-expansion. *SIAM Journal on Control and Optimization*, 36(6):1937–1939, 1998.

[13] K.-H. Elster. *Modern Mathematical Methods of Optimization.* Akademie Verlag, Berlin, 1993.

[14] B Gompertz. On the nature of the function expressive of the law of human mortality. *Phil Trans Royal Soc*, 115(513-585), 1825.

[15] E. H. Hixon. Prediction of facial growth. *Report of the Congress of the European Orthodontic Society*, 44:127–139, 1968.

[16] W. J. Houston. The current status of facial growth prediction – a review. *British Journal of Orthodontics*, 6:11–17, 1979.

[17] W. J. B. Houston and W. A. B. Brown. Family likeness as a basis for facial growth prediction. *Eur. J. Orthod.*, 2:13 – 18, 1980.

[18] R. M. Jenss and N. Bayley. A mathematical method for studying the growth of a child. *Human Biology*, 9:556–563, 1937.

[19] J. Kallrath, J. P. Schloeder, and H. G. Bock. Least squares parameter estimation in chaotic differential equations. *Celest. Mech. Dyn. Astron.*, 56:353–371, 1993.

[20] H. Kantz, J. Kurths, and G. Mayer-Kress, editors. *Nonlinear Analysis of Physiological Data*. Springer-Verlag, 1998.

[21] H. Kantz and T. Schreiber. *Nonlinear time series analysis*. Number 7 in Cambridge Nonlinear Science Series. Camebridge University Press, 1997.

[22] K. Karhunen. Zur spektralen Theorie stochastischer Prozesse. *Ann. Acad. Sci. Fenn. A1, Math. Phys. 37*, 1946.

[23] R. S. Lee, F. J. Daniel, M. Swartz, S. Baumrind, and E. L. Korn. Assessment of a method for the prediction of mandibular rotation. *American Journal of Orthodontics and Dentofacial Orthopedics*, 91:395–402, 1987.

[24] S. Lele. Some comments on coordinate-free and scale-invariant methods in morphometrics. *American Journal of Physical Anthropology*, 85:407–417, 1991.

[25] S. Lele and J. T. Richtsmeier. Euclidean distance matrix analysis: A coordinate-free approach for comparing biological shapes using landmark data. *American Journal of Physical Anthropology*, 86:415–427, 1991.

[26] M. Loève. Fonctions aléatoires de second ordre. *C.R. Acad. Sci. Paris*, 1946.

[27] E. Marubini, L. F. Resele, J. M. Tanner, and R. H. Whitehouse. The fit of Gompertz and logistic curves to longitudinal data during adolescence on height, sitting height and biacromial diameter in boys and girls of the Harpenden growth study. *Human biology*, 44(3):511–523, 1972.

[28] M. L. Moss, R. Skalak, H. Patel, K. Sen, L. Moss-Salentijn, M. Shinozuka, and H. Vilmann. Finite element method modeling of cranifacial growth. *American Journal of Orthodontics*, 87:453–474, 1985.

[29] R. E. Moyers and F. L. Bookstein. The inappropriateness of conventional cephalometrics. *American Journal of Orthodontics*, 75(6):599ff., 1979.

[30] R. S. Nanda. The rates or growth of several facial components measured from serial cephalometric roentgenograms. *American Journal of Orthodontics*, 41:658–673, 1955.

[31] W. Press, S. Teukolsky, W. Vetterling, and B. Flannery. *Numerical Recipes in C*. Cambridge University Press, Cambridge, New York, 1992.

[32] F. J. Rohlf and L. F. Marcus. A revolution in morphometrics. *TREE*, 8:129–132, 1993.

[33] J. Rübel, J. Starke, and C. J. Lux. Analysis and visualization of craniofacial growth - a longitudinal study using rat calvarial data. In *Proceedings of the 16th IMACS World Congress*. IMACS, August 2000.

[34] J. Stoer and R. Bulirsch. *Numerische Mathematik 2*. Springer, 1990. 3. Auflage.

[35] J. M. Tanner. The human growth curve. In J. M. Tanner and N. A. Barnicot, editors, *Human Biology*. Oxford University Press, New York, 1964.

[36] J. M. Tanner, R. H. Whitehouse, and M. Takaishi. Standards from birth to maturity for height, weight, height velocity, and weight velocity: British children, 1965. *Archives of disease in childhood*, 41(219):454–471, 1966.

[37] J. Timmer, H. Rust, W. Horbelt, and H. U. Voss. Parametric, nonparametric and parametric modelling of a chaotic circuit time series. *Physics Letters A*, 274:123–34, 2000.

[38] C. Uhl. *Analyse raumzeitlicher Daten strukturbildender Systeme*. PhD thesis, Universität Stuttgart, Verlag Shaker, Aachen, 1995.

[39] C. Uhl, R. Friedrich, and H. Haken. Analysis of spatiotemporal signals of complex systems. *Physical Review E*, 51(5):3890–3900, 1995.

[40] S. L. Zeger and S. D. Harlow. Mathematical models from laws of growth to tools for biologic analysis: Fifty years of *Growth*. Growth, *51:1–21, 1987.*

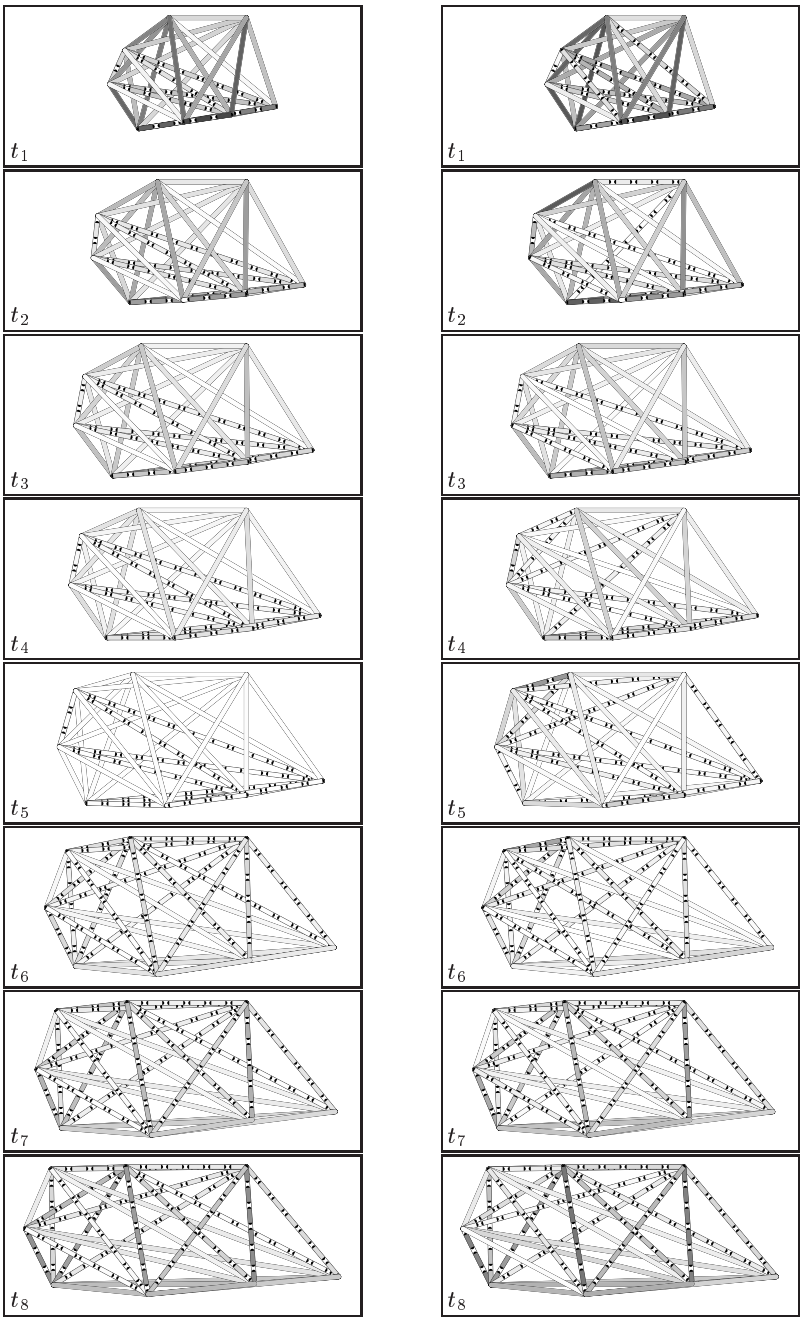

Figure 5. Visualization of the second mode with mode coefficient $\xi_2(t_k)v^{(2)}$ (left) and the entire shape component, i.e., the sum of all but the first mode with mode coefficients $\sum_{i=2}^{n} \xi_i(t_k)v_j^{(i)}$ of the KLD for rat no. 2 of the Vilman rat data set. The gray shades of the interlandmark distances, computed by $\xi_2(t_k)v_j^{(2)}/q_j(t_k)$ and $\sum_{i=2}^{n} \xi_i(t_k)v_j^{(i)}/q_j(t_k)$ respectively for $t_1, \ldots, t_8$, show the degree of deviation from the mean form, where dashed lines stand for a negative contribution of the modes and mode coefficients and solid lines for positive ones.

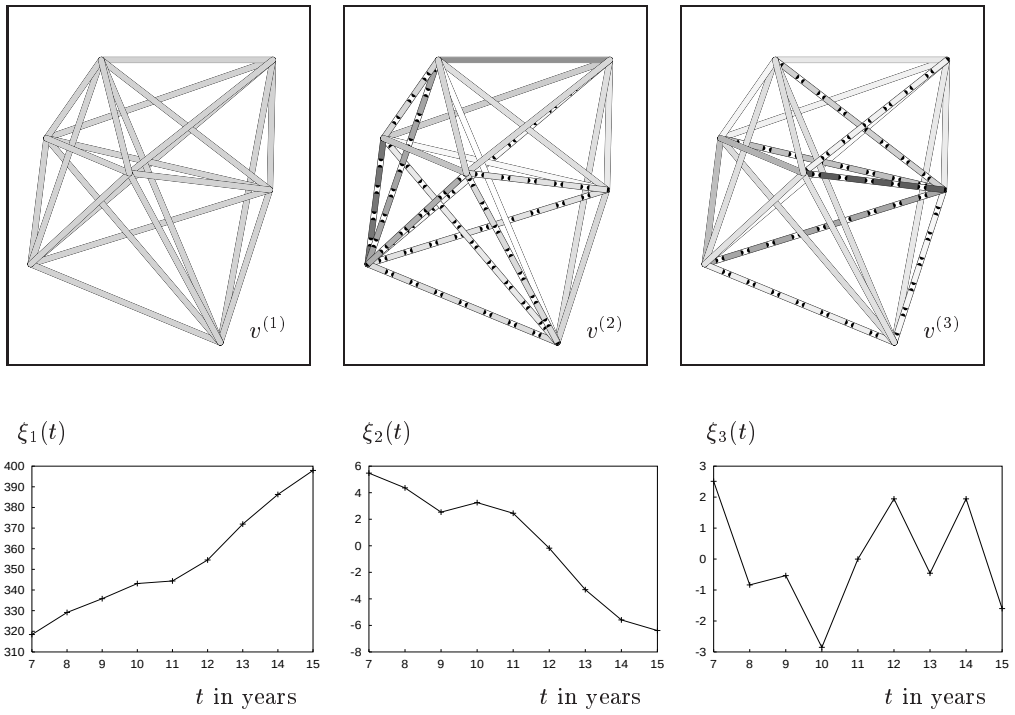

Figure 6. Modes v_1, v_2, v_3 of proband no. 4 of the Belfast Growth Study with the corresponding eigenvalues $\lambda_1 = 0.999823728$, $\lambda_2 = 0.000125172$, $\lambda_3 = 0.000019319$.

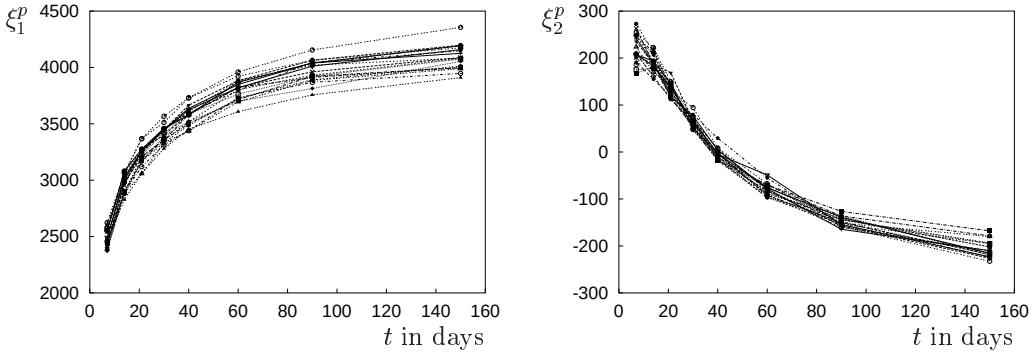

Figure 7. The coefficients ξ_1^p (left) and ξ_2^p (right) of the first and second KLD-mode for all rats p from the Vilman data set plotted over time.

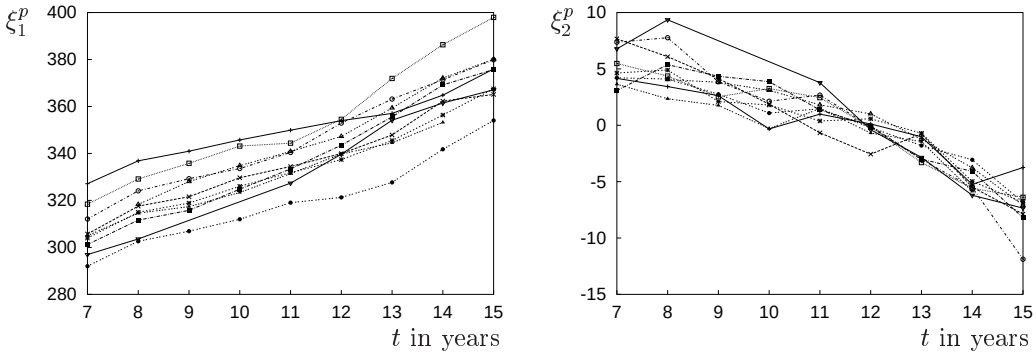

Figure 8. The coefficients ξ_1^p (left) and ξ_2^p (right) of the first and second KLD-mode for all probands p selected from the Belfast Growth Study plotted over the time. Compared with the rat calvarial data in Fig. 7 the human probands show a larger relative variation in shifts of the probands' graphs to each other.

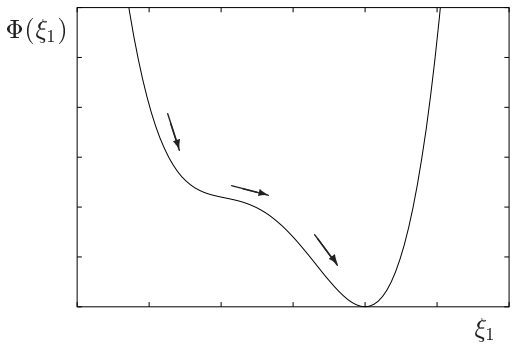

Figure 9. Potential $\Phi(\xi_1)$ of order 4 to model the size-growth by a gradient descent flow.

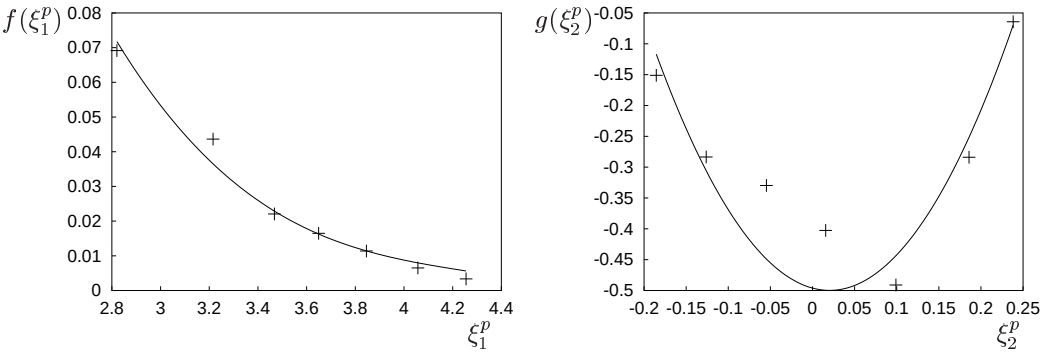

Figure 10. The fit of the model (3) and (4) to the growth dynamics of the mode coefficients ξ_1^p (left) and ξ_2^p (right) of the first and second KLD mode for the example of rat no. 17 from the Vilman data set.

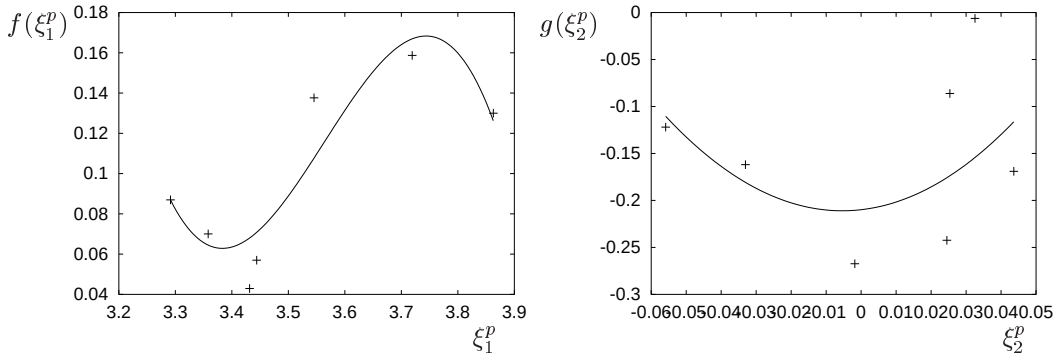

Figure 11. The fit of the model (3) and (4) to the growth dynamics of the mode coefficients ξ_1^p (left) and ξ_2^p (right) of the first and second KLD mode for proband no. 4 of the Belfast Growth Study.

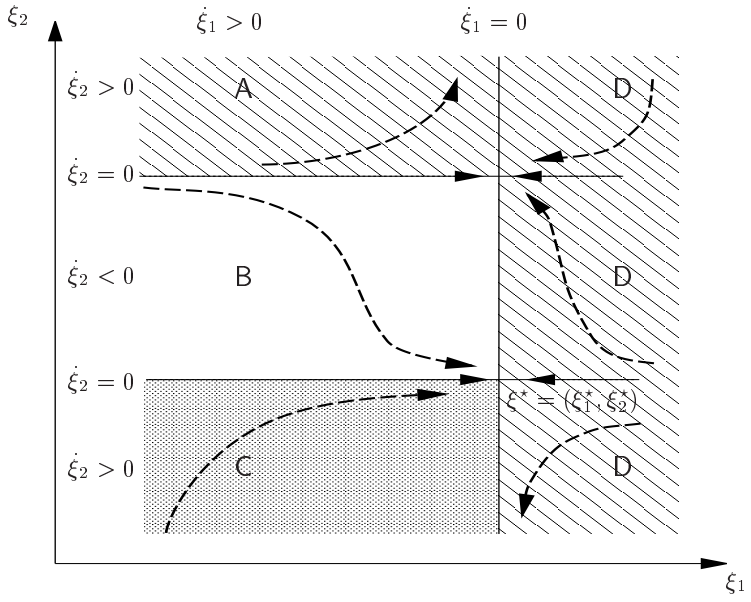

Figure 12. Flow of the vector field (13) with parameters given in tables 1 and 2. The upper and right hatched area marked with "A" and "D" contain medically impossible states and are not reached if the initial values are chosen outside. The states in the lower hatched area marked with "C" are avoided by sign convention of ξ_2 and $v^{(2)}$ in the product $\xi_2 v^{(2)}$.

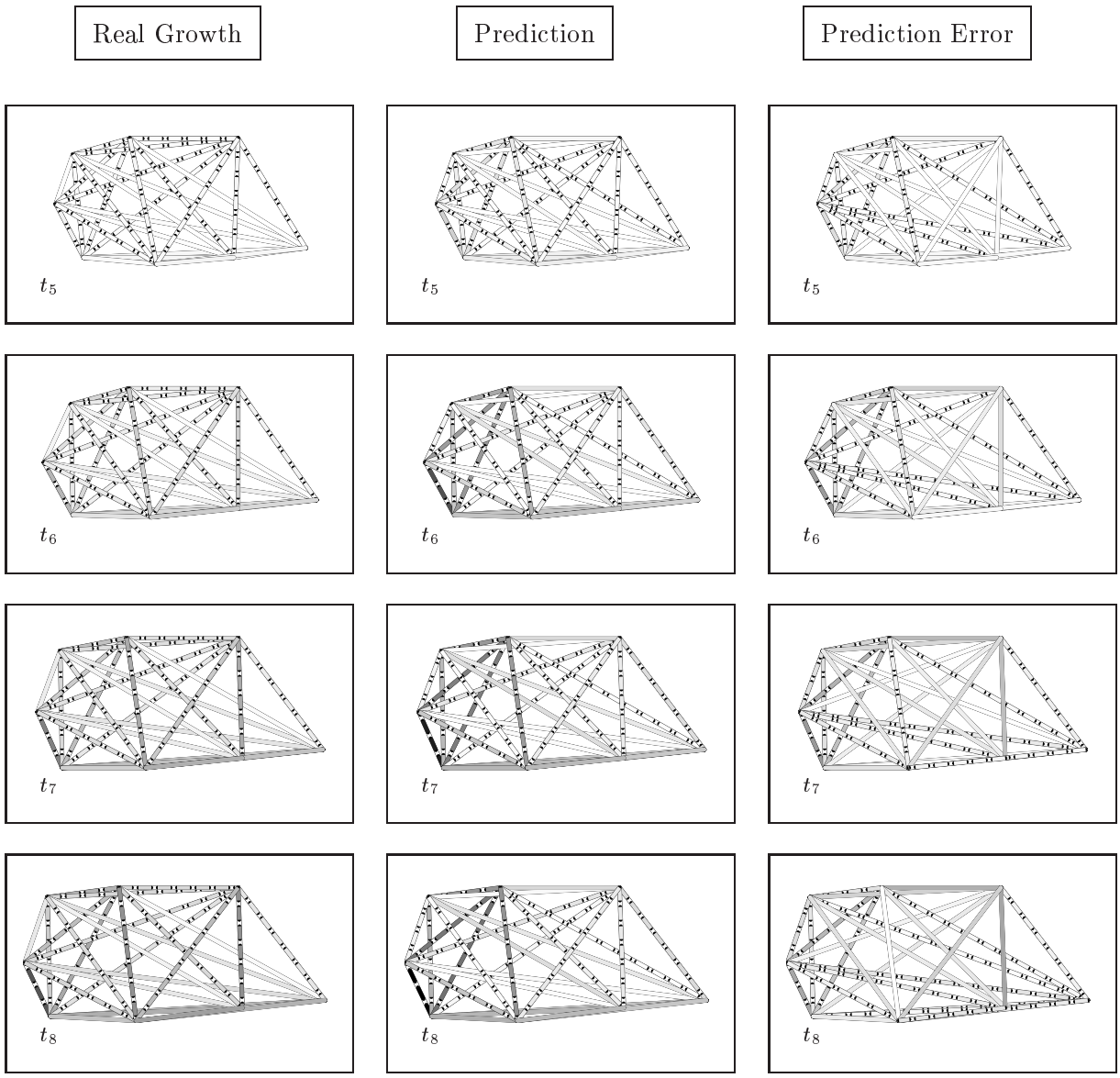

Figure 13. Comparison of $\xi_2(t)v^{(2)}$ of the real growth of rat no. 17 shown on the left with the prediction results $\tilde{\xi}_2(t)\tilde{v}^{(2)}$ in the middle and the prediction error on the right for times t_5 to t_8. The data of the times t_4 and t_5 was used as basis for the prediction.

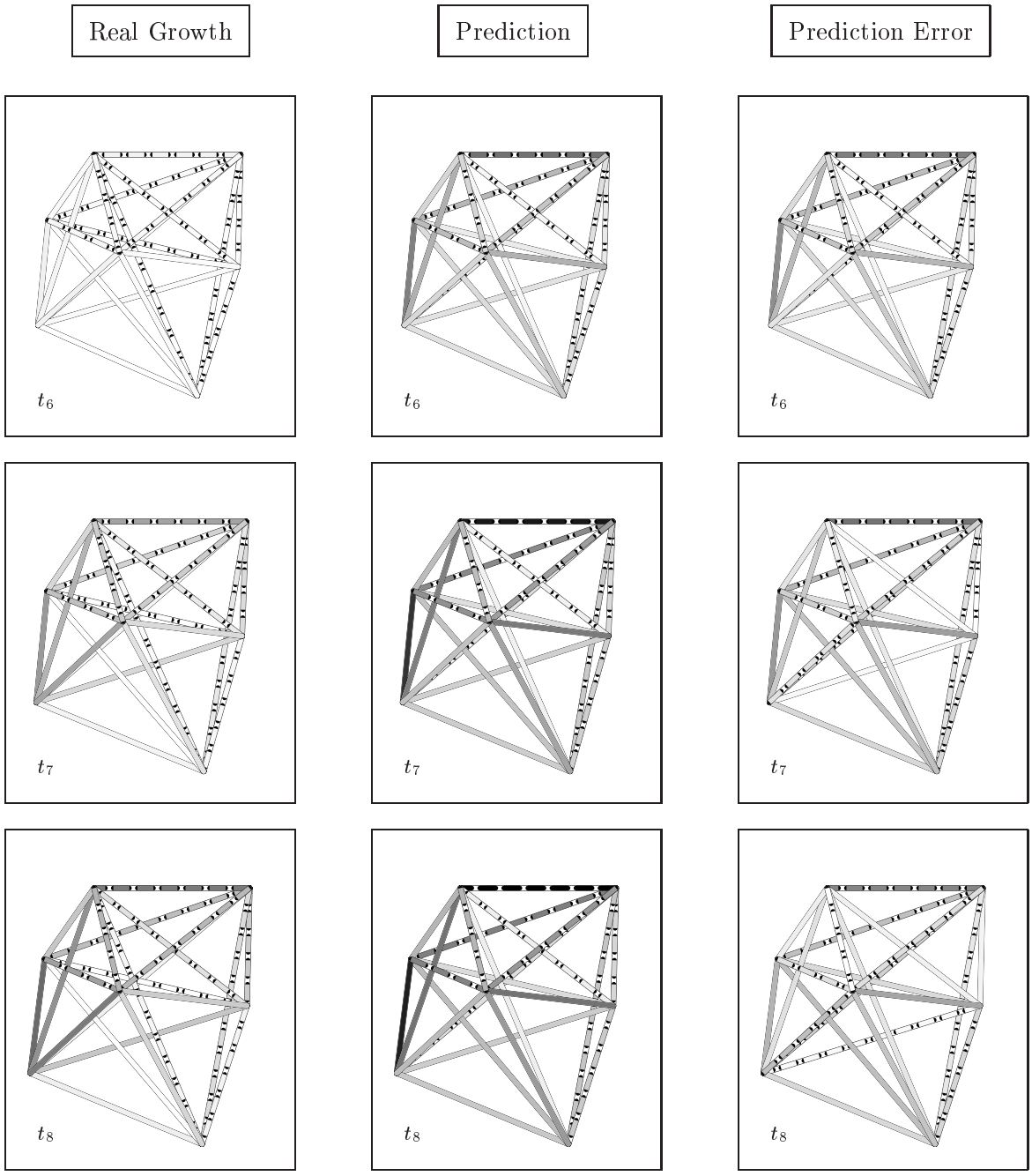

Figure 14. Comparison of $\xi_2(t)v^{(2)}$ of the real growth of proband no. 4 of the Belfast Growth Study shown on the left, with the prediction results $\tilde{\xi}_2(t)\tilde{v}^{(2)}$ in the middle and the prediction error on the right. The data of ages 11–13 years was used as basis for the prediction of the ages 14 and 15 (times t_7 to t_8).

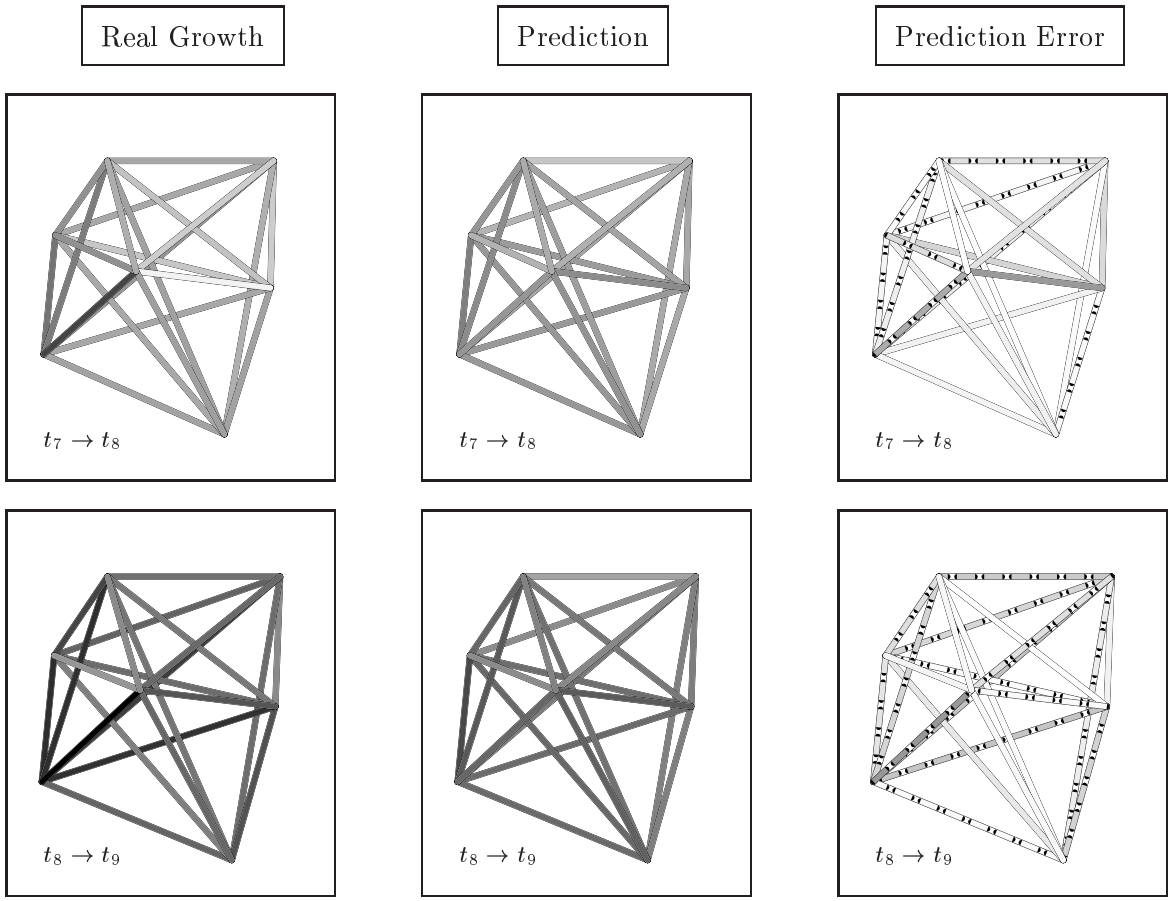

Figure 15. Relative changes of the real growth of proband no. 4 from ages 13 to 14 and 14 to 15, compared with the predicition result which is based on the ages 11–13 years. The prediction error as difference of both relative changes is shown on the right. The corresponding states are shown in Fig. 14.

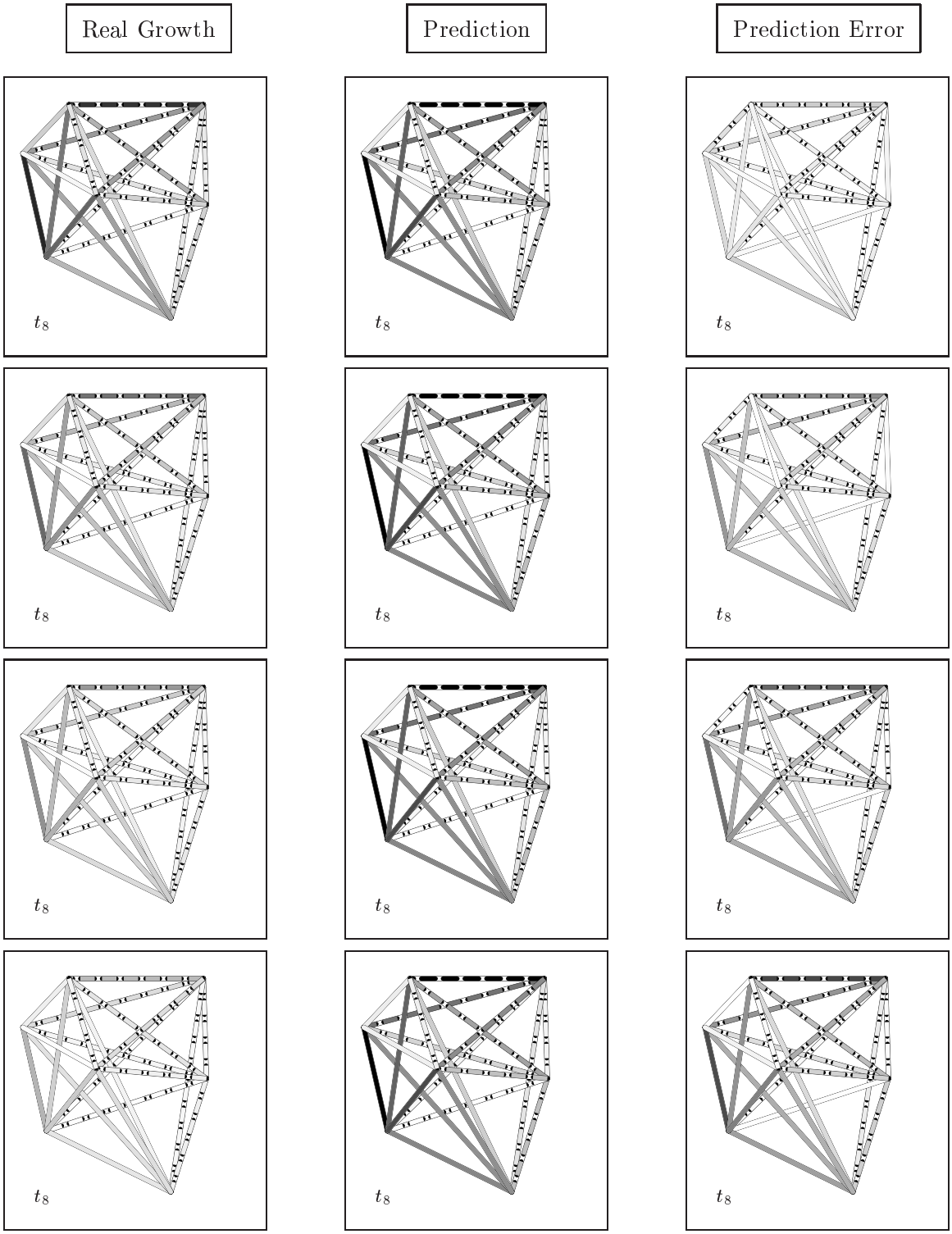

Figure 16. Comparison of $\xi_2 v_2$ of the Real growth (left) compared with the prediction (middle) for a proband who has not been included into the data set for determination of the model parameters. The prediction error is depicted on the right. The means over the 9 subjects were used as individual parameters. The ages 7–14 years were used as basis for the prediction. The column in the middle shows prediction results for the age 15 with different individual time scales $\alpha_2 = \{\bar{\alpha}/16, \bar{\alpha}/4, \bar{\alpha}/2, \bar{\alpha}\}$ with mean $\bar{\alpha} = 3.180$. The growth pattern of the second mode is qualitatively well predicted. The quantitatively best prediction is given for $\alpha_2 = \bar{\alpha}/16$ (first row).